The Astrophysical Journal, 865:69 (10pp), 2018 September 20 https://doi.org/10.3847/1538-4357/aad867
© 2018. The American Astronomical Society. All rights reserved.

Elemental Composition at the Cosmic-Ray Source Derived from the *ACE*-CRIS Instrument. I. $_6$C to $_{28}$Ni

M. H. Israel[1], K. A. Lave[1,5], M. E. Wiedenbeck[2], W. R. Binns[1], E. R. Christian[3], A. C. Cummings[4], A. J. Davis[4], G. A. de Nolfo[3], R. A. Leske[4], R. A. Mewaldt[4], E. C. Stone[4], and T. T. von Rosenvinge[3]
[1] Department of Physics & the McDonnell Center for the Space Sciences, Washington University, St. Louis, MO 63130, USA; mhi@wustl.edu
[2] Jet Propulsion Laboratory, California Institute of Technology, Pasadena, CA 91109, USA
[3] NASA Goddard Space Flight Center, Greenbelt, MD 20771, USA
[4] California Institute of Technology, Pasadena, CA 91125, USA
Received 2018 January 29; revised 2018 July 16; accepted 2018 August 3; published 2018 September 21

Abstract

We report new elemental source abundances from $_6$C to $_{28}$Ni for galactic cosmic rays, using observations from the Cosmic Ray Isotope Spectrometer (CRIS) on board the NASA *Advanced Composition Explorer* spacecraft. Abundances were calculated using CRIS energy spectra at energies below 550 MeV/nucleon from the 1997–98 and 2009–10 solar-minimum periods, as well as from the 2001–03 solar-maximum period. These new results, when combined with results for heavier elements reported in a forthcoming paper, are consistent with a model of galactic cosmic-ray origin where nuclei found in interstellar grains are accelerated preferentially over those found in interstellar gas, with this acceleration happening in OB associations.

Key words: astroparticle physics – cosmic rays – ISM: abundances

1. Introduction

The relative abundances of elements at the cosmic-ray source give information about where the cosmic rays originate and the mechanisms by which they are accelerated. Rauch et al. (2009) have shown that the acceleration process differentiates between elements that are found in interstellar grains (refractory elements) and those found in the interstellar gas phase (volatile elements) and that the cosmic-ray source composition is consistent with an origin in OB associations. Those conclusions were drawn using data from the balloon-borne Trans-Iron Galactic Element Recorder (TIGER) for elements with atomic number (Z) in the interval $26 \leqslant Z \leqslant 38$, combined with data from the C2 instrument on the third *High Energy Astronomy Observatory* (*HEAO3*) for $Z \leqslant 26$.

The Cosmic Ray Isotope Spectrometer (CRIS; Stone et al. 1998a) is one of nine instruments on board the *Advanced Composition Explorer* (*ACE*) spacecraft (Stone et al. 1998b) located in a halo orbit about the L1 Lagrangian point, 1.5 million kilometers sunward from Earth. CRIS measures the nuclear charge, mass, and incident energy of cosmic rays using the multiple-dE/dx versus total-energy technique. CRIS has a large geometrical acceptance of $\sim$250 cm^2 sr and excellent charge and mass resolution.

The CRIS instrument has been operating in space since 1997 August, giving high-precision data on cosmic-ray nuclei at 1 au from the Sun in the ecliptic plane. It is designed to measure the elemental and isotopic composition of ions from He to Ni ($2 \leqslant Z \leqslant 28$) at energies between $\sim$50 and $\sim$550 MeV/nucleon (Stone et al. 1998a). In particular, during 2009 and early 2010, solar modulation of the cosmic rays was less pronounced than it has been at any previous solar minimum since the start of the space age (Mewaldt et al. 2010), and thus has yielded data less affected by solar modulation than any previous measurement at similar energies near Earth (Lave et al. 2013). In this paper we take these observed elemental abundances and estimate the abundances at the galactic cosmic-ray (GCR) source.

Inferring cosmic-ray source abundances from observations near Earth requires a model of cosmic-ray propagation in the interstellar medium and a model of cosmic-ray modulation in the interplanetary medium of the heliosphere. The interstellar model accounts for fragmentation of cosmic-ray nuclei as a result of nuclear interactions with nuclei in the interstellar medium, as well as for radioactive decay; these are processes that produce secondary cosmic-ray nuclei. It also accounts for leakage of the cosmic rays out of the Galaxy and for energy loss (and possibly for reacceleration) in the interstellar medium. The interplanetary model takes account of the loss and spread of the energies of the cosmic rays as they interact with the magnetic field carried by the expanding solar wind.

We have applied a leaky-box steady-state model of interstellar propagation and a spherically symmetric model of modulation in the heliosphere to infer cosmic-ray source abundances from the CRIS observations, and we have also used the same models to infer source abundances from the HEAO3-C2 observations (Engelmann et al. 1990). For the modeling of interstellar propagation, we used an updated database of nuclear interaction cross sections (Lave 2012). We have also analyzed the uncertainties in the derived cosmic-ray source abundances resulting from uncertainties in these cross sections and in other parameters describing these models. Those uncertainties are important in view of the excellent charge resolution and statistics of the observations. Our results here, when combined with results for heavier elements reported in a forthcoming paper (Binns et al. 2018), support the earlier conclusions about the cosmic-ray source described by Rauch et al. (2009) and by Binns et al. (2007).

2. Observations

The data from CRIS used for this study are taken from Lave et al. (2013), and details of the data analysis are described in that paper. There we reported the observed elemental energy

[5] Current address for K.A. Lave: Maryville University, St. Louis, MO 63141.

spectra of all GCR species with nuclear charge $5 \leqslant Z \leqslant 28$ in Z-dependent energy ranges between 50 and 550 MeV/nucleon for three time periods during solar cycles 23 and 24. Data used there come from two periods of minimum solar activity (i.e., maximum GCR intensities), one in 1997–1998 and the other in 2009–2010, and from a period of maximum solar activity (minimum GCR intensities) in 2001–2003.

3. Derivation of Source Abundances

For elements whose observed abundances include a non-negligible primary component (which we designate as "group 1") —C, N, O, Ne, Na, Mg, Al, Si, S, Ar, Ca, Fe, Co, Ni—we derive abundances at the cosmic-ray source from our CRIS observations by a standard matrix-inversion least-squares fitting to their observed intensities and statistical uncertainties at seven energies (Lave et al. 2013). The process for this derivation is described in detail in Appendix A. This process simultaneously gives source abundances and their statistical uncertainties. For elements whose observed cosmic-ray abundances are overwhelmingly secondary (which we designate as "group 2")—F, P, Cl, K, Sc, Ti, V, Cr, and Mn (Wiedenbeck et al. 2007)—we made no attempt to derive source abundances; rather, we assumed (see Table 4 in Appendix B) that the abundance ratio of each of these elements to nearby dominantly primary elements was equal to the corresponding ratio found in the solar system (Lodders et al. 2009). For this work, we made no attempt to derive isotopic source abundances; rather we assumed that each element, except Ne, had relative isotopic abundances at the source that were the same as the solar system isotopic abundances (Lodders et al. 2009). For Ne, we assumed a source with $^{22}\mathrm{Ne}/^{20}\mathrm{Ne} = 0.387$, as derived from CRIS isotopic measurements (Binns et al. 2005); this ratio is five times the ratio found in the solar wind. In fact, this overabundance of ^{22}Ne gave early evidence for a cosmic-ray origin in OB associations (Higdon & Lingenfelter 2003; Binns et al. 2005, 2007).

We thus derived source abundances using four selected sets of spectra observed near Earth: three by CRIS (Lave et al. 2013) (1) during the solar-minimum period 1997 December 5 to 1998 April 20, (2) during the solar-maximum period 2001 May 1 to 2003 September 1, (3) during the recent solar-minimum period 2009 March 23 to 2010 January 13, and one by HEAO3-C2 (Engelmann et al. 1990) during the period 1979 October 17 to 1980 June 12. As described below in Section 4, these four sets of observations do not yield identical source abundances; the differences are indicative of systematic uncertainties introduced by our models of interstellar propagation and modulation in the heliosphere.

3.1. Interstellar Propagation

Observed cosmic-ray nuclides are a mixture of primary nuclides accelerated at the cosmic-ray source and secondary nuclides produced in interstellar space by fragmentation of heavier nuclides interacting with nuclei of interstellar material and by radioactive decay. We used a leaky-box interstellar propagation model based on the formalism of Meneguzzi et al. (1971) to take an assumed set of elemental abundances at the source and derive propagated steady-state interstellar abundances. In this propagation model Λ^{esc}, the energy-dependent mean free path (mfp) for escape from the Galaxy, is of the form (Soutoul & Ptuskin 1999; Davis et al. 2000)

$$\Lambda^{\mathrm{esc}} = \frac{C_0\beta}{\left(\frac{\beta R}{C_1}\right)^{C_2} + \left(\frac{\beta R}{C_3}\right)^{C_4}},$$

where R is particle rigidity, β is particle speed divided by the speed of light, and $C_0 = 32.45\ \mathrm{g\,cm^{-2}}$, $C_1 = 0.90$ GV, $C_2 = 0.59$, $C_3 = 1.17$ GV, $C_4 = -1.60$ (Lave et al. 2013).

This escape mfp peaks at $\sim$13 g cm^{-2} at $\sim$750 MeV/nucleon (for mass-to-charge ratio = 2) and falls to $\sim$6 g cm^{-2} at $\sim$200 MeV/nucleon and at $\sim$7.5 GeV/nucleon, as plotted in Figure 5 of Lave et al. (2013). (This escape mfp is not valid for interstellar energies below $\sim$200 MeV/nucleon.) Lave et al. (2013) found the parameters of the model by minimizing the reduced-chi-squared values for the fits of the transport model to the measured ratio of boron to carbon and to the measured ratio of the iron-secondary group, $_{21}$Sc + $_{22}$Ti + $_{23}$V, to iron.

3.2. Solar Modulation

To derive the spectra that would be observed near Earth from the calculated interstellar spectra requires accounting for the diffusion, convection, and adiabatic deceleration of the cosmic rays in the interplanetary magnetic field carried by the solar wind. We use a spherically symmetric Fokker–Plank equation (Goldstein et al. 1970) with the Crank–Nicholson technique discussed by Fisk (1971), as described by Lave et al. (2013). We use the full solution of the Fokker–Plank equation, not the force-field approximation (Gleeson & Axford 1968); nonetheless, there is a "modulation potential," ϕ, that conveniently characterizes the level of solar modulation. (For a definition of ϕ see Section 6.2 of Lave et al. 2013.) For each of the three sets of CRIS data, we determined an appropriate level of modulation by finding the level that gave the best match between the calculated and the observed spectra of five primary elements, C, O, Mg, Si, and Fe, using CRIS data averaged over 27-day Bartels rotations (Wiedenbeck et al. 2005). For any particular time period, the levels thus derived from each of these elements are in close, but not perfect, agreement, as shown in Figure 1, and we used the mean of the values of ϕ derived from these five elements. The values of ϕ thus derived for the three selected CRIS observation periods are: (1) 1997–98: 325 MV; (2) 2001–03: 900 MV; (3) 2009–10: 250 MV. For the HEAO3-C2 observation period we derived $\phi = 750$ MV using the same procedure with the HEAO3-C2 spectra.

3.3. Calculated Spectra at Earth

The solid curves in Figure 2 show the spectra near Earth that we calculated for the fourteen "group 1" elements for each of the three selected time periods of CRIS data. These calculations used the interstellar propagation described above in Section 3.1, the solar modulation described in Section 3.2, and the determination of source abundances of these fourteen elements described in detail in Appendix A. These calculations assumed an injection spectrum at the cosmic-ray source that is a power law in momentum with a spectral index of −2.35. Also shown as data points in Figure 2 are the intensities measured by CRIS at each of seven energies. The error bars on these points indicate statistical uncertainties only; in

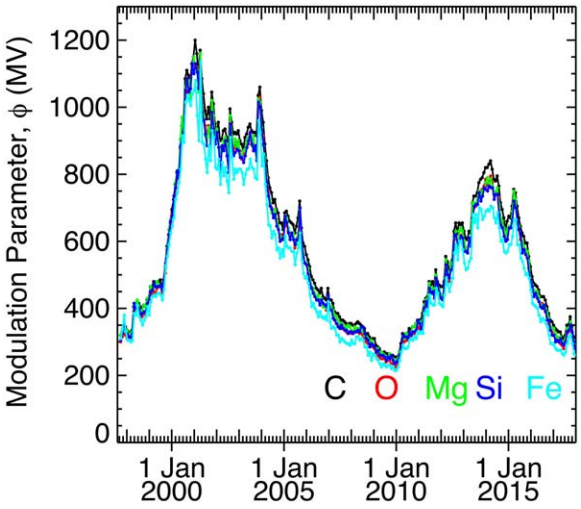

Figure 1. Modulation parameter, ϕ, derived by finding the value that results in the best fit between the calculated near-Earth spectrum and the data, averaged over each 27-day Bartels rotation, for each of five abundant primary elements —carbon, oxygen, magnesium, silicon, and iron.

many cases these error bars are smaller than the data points. We note the good agreement between the calculations and the data.

4. Derived Source Abundances

4.1. Abundances Derived from CRIS Data

Table 1 displays source abundances derived from CRIS data in each of the three selected observation periods. Abundances of various elements are given relative to the abundance of Si defined as 1000. In this table the uncertainty associated with each element is only the statistical uncertainty. Systematic uncertainties on the 2009–10 data are tabulated in Table 2.

The source abundances derived from the two sets of CRIS solar-minimum data are close to one another, but the differences between them are not fully accounted for by statistical uncertainties. We have looked at the ratio of the source abundances from the two minima (Figure. 3(a)) and compared them to unity. The reduced chi-squared is 4.2, indicating a lack of good agreement. We suggest that these differences may result from the fact that we use the same spherically symmetric model of solar modulation in both periods, even though the polarity of the solar magnetic field reversed between these two minima. The consequent differences in cosmic-ray transport due to gradient and curvature drifts in the interplanetary medium are not accounted for in this modulation model.

For the remainder of this report, we take as our best result for the source abundances those derived from the second solar-minimum period, 2009 March 23–2010 January 13. During this period the depth of the modulation was less than that in our earlier period, and indeed was less than that for any other solar minimum during which measurements have been made outside the atmosphere (Mewaldt et al. 2010). Thus, these observations were closer to interstellar values than any previous observations made in the inner solar system. Furthermore, the combination of higher cosmic-ray intensities and a longer solar-minimum observation period gave us better statistical precision during this 2009–10 period than during the earlier period.

We note that most of the abundances we derive from the solar-maximum period (2001–03) disagree with our 2009–10 solar-minimum abundances by more than the statistical uncertainties, and indeed the reduced chi-squared for the fit of the ratios in Figure 3(b) to unity is 23.4, confirming the visual impression of poor agreement. The principal difference between these two calculations is the level of solar modulation, 250 MV versus 900 MV, so the difference in derived source abundances appears to confirm the inadequacy of our solar-modulation model, especially in periods of strong modulation. However, we note that the largest differences between the solar-minimum and solar-maximum calculated source abundances are in elements that have substantial secondary contributions. Thus, the differences between these two sets of derived source abundances may result from incorrect estimates of the energy dependence of interaction cross sections or of the mean free path for escape from the Galaxy used for interstellar propagation, since adiabatic deceleration in the solar wind is greater at solar maximum than at solar minimum (Niebur et al. 2003), so the interstellar energies of the cosmic rays observed by CRIS during solar maximum are greater by a few hundred MeV/nucleon (and thus closer to the energy at which the leakage mean free path from the Galaxy in our propagation model is maximum) than the interstellar energies of those observed by CRIS during solar minimum.

4.2. Systematic Uncertainties of Source Abundances Derived from CRIS

Calculated systematic uncertainties of our source abundances are shown in Table 2. Columns 2 and 3 of Table 2 are identical with the rightmost columns of Table 1. Column 4 shows the uncertainties in our source abundances that are attributable to systematic uncertainties in the CRIS measurement of near-Earth energy spectra, which vary between 2.9% for our lowest energy $_{6}$C to 9.3% for our highest energy $_{28}$Ni. This systematic uncertainty is the quadratic combination of a 2% uncertainty attributed to the geometrical acceptance of the CRIS instrument, a 2% uncertainty attributed to the hodoscope efficiency, and a range- and charge-dependent uncertainty attributed to the correction for fragmentation of nuclei in the detector system, as described by Lave et al. (2013). The procedure for obtaining the source abundance uncertainty from the measurement uncertainty is analogous to that used for the statistical uncertainties as discussed in Appendix A.

Columns 5–8 list the systematic uncertainties in the derived source abundances arising from uncertainties in the propagation and modulation model parameters. These source uncertainties were obtained by repeating the abundance calculations after changing one of several parameters at a time. Column 5 shows the change in derived source abundances due to a $\pm$25 MV change in the modulation parameter ϕ. Column 6 shows the change in source abundances that would result from an assumed $\pm$20% change in all the partial cross sections, assuming that the changes in all those cross sections are completely correlated. Our use of 20% is based on our estimate of typical uncertainties in the combination of experimental and semi-empirical cross sections that we employed.

Changes in partial cross sections produce a substantially larger change in the source abundances if the cross-section changes are completely correlated than if they are perfectly uncorrelated. (Hinshaw & Wiedenbeck 1983; see Appendix B.) In most of our work (unless otherwise indicated) we have

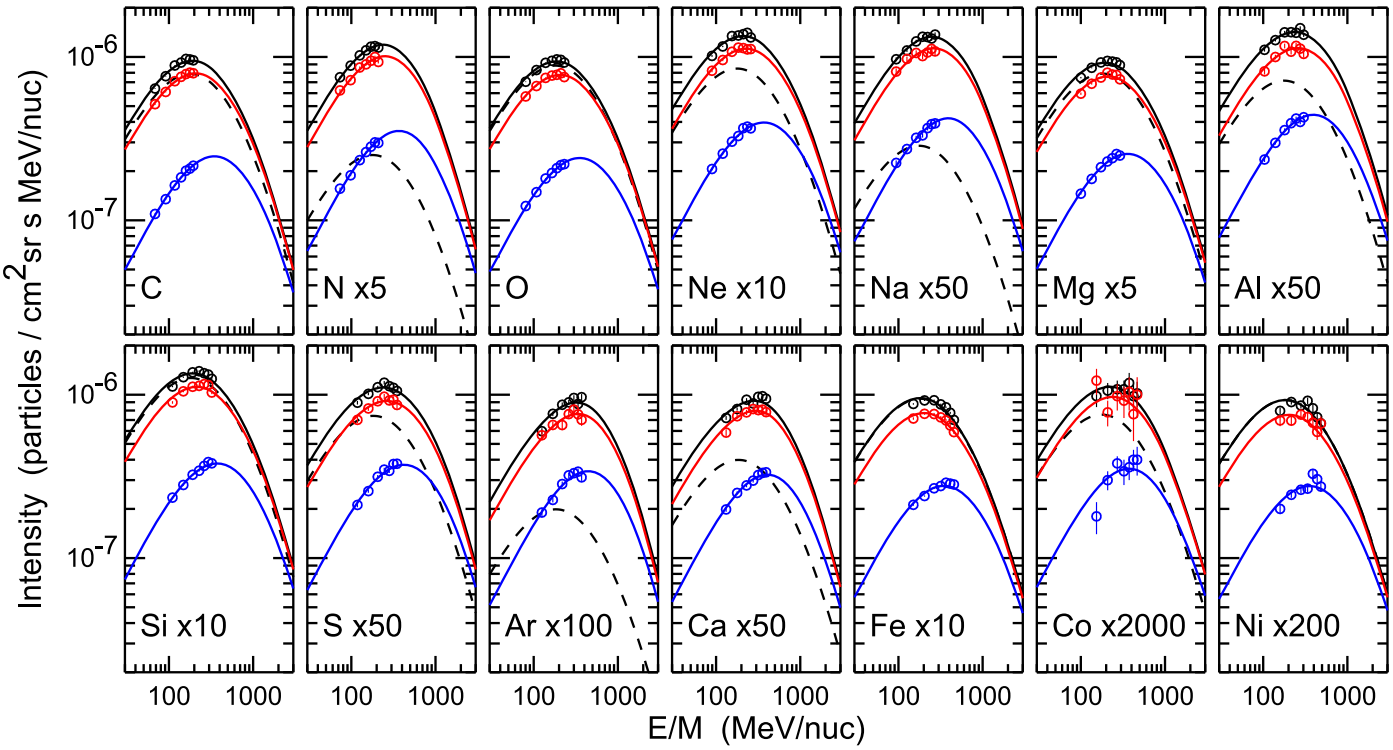

Figure 2. Comparison between observed near-Earth intensities (points) and calculated spectra (solid curves). Upper (black) curve and data: 2009–10 solar minimum. Middle (red) curve and data: 1997–98 solar minimum. Lower (blue) curve and data: 2001–03 solar maximum. The dashed curve is the primary component of the calculated 2009–10 curve. (For elements with a negligible secondary component (Fe and Ni) the dashed curve is hidden under the solid upper (black) curve.)

Table 1
Source Abundances Relative to Si = 1000 Derived from CRIS Data, with 1σ Statistical Uncertainties

	1997 Dec 5–1998 Apr 20 Solar Minimum	2001 May 1–2003 Sep 1 Solar Maximum	2009 Mar 23–2010 Jan 13 Solar Minimum
$_{6}$C	3739.9 ± 14.6	3598.5 ± 12.2	3677.3 ± 8.5
$_{7}$N	244.1 ± 7.7	206.3 ± 6.8	256.4 ± 4.4
$_{8}$O	4871.7 ± 15.2	4653.4 ± 12.1	4837.3 ± 8.9
$_{10}$Ne	508.7 ± 6.0	497.2 ± 4.9	511.0 ± 3.5
$_{11}$Na	35.7 ± 2.8	26.6 ± 2.3	37.2 ± 1.6
$_{12}$Mg	1106.7 ± 7.6	1095.3 ± 5.9	1111.2 ± 4.5
$_{13}$Al	89.2 ± 2.9	88.3 ± 2.4	103.9 ± 1.8
$_{14}$Si	1000.0 ± 6.9	1000.0 ± 5.3	1000.0 ± 4.2
$_{16}$S	123.1 ± 3.0	126.2 ± 2.4	128.8 ± 1.8
$_{18}$Ar	16.0 ± 2.0	15.1 ± 1.7	18.6 ± 1.2
$_{20}$Ca	82.5 ± 3.1	72.8 ± 2.5	81.2 ± 1.9
$_{26}$Fe	1010.5 ± 6.9	1054.7 ± 4.9	1037.3 ± 4.3
$_{27}$Co	4.5 ± 0.6	3.9 ± 0.4	4.4 ± 0.4
$_{28}$Ni	56.1 ± 1.7	60.3 ± 1.2	57.3 ± 1.0

chosen to assume the worst case and use a completely correlated 20% change in the partial cross sections. Column 7 shows the change due to a ±5% change in all the total cross sections. Column 8 shows the effect of a ±10% energy-independent change in the mean free path for escape from the Galaxy. Column 9 is the quadratic sum of columns 3 through 8; this is our conservative estimate of the uncertainty, statistical plus systematic, of our CRIS source abundances in column 2. (Column 10 is described below, after the discussion of Figure 4.)

Figure 4 illustrates the various contributions to the fractional uncertainties of these CRIS solar-minimum source abundances for each element. We note that the excellent statistics of the data leave us with overall uncertainty dominated by systematic uncertainties, primarily uncertainties in the model used for deriving the sources from the observations.

Throughout this paper, we use the total statistical and systematic uncertainty shown in column 9 of Table 2, in which the systematic uncertainty on the partial cross sections assumed perfectly correlated 20% changes. For reference, we show in column 10 what the total statistical and systematic uncertainty would be if the uncertainties in partial cross sections were completely uncorrelated. (See Appendix B.) For the elements that have relatively small secondary components, the differences between these two combined uncertainties are small. We note that the tabulated uncertainties are quite substantial for elements that have a significant secondary contribution to the observed data—notably N, Na, Ar, Ca, and Co. These systematic uncertainties are dominated by our estimate of the uncertainty in the partial cross sections for production of these elements. An analysis of the isotopic results from CRIS will result in smaller source uncertainties for some of these elements. A preliminary analysis of those isotopic results has been reported by Wiedenbeck et al. (2007).

4.3. Comparison with Source Abundances Derived from Other Instruments

A widely used set of source abundances has been that derived by Engelmann et al. (1990) using data from the C2 instrument on the *HEAO3* spacecraft. Those data were taken during a period of solar modulation intermediate between solar minimum and solar maximum. From the shape of their spectra, we derive a value of the modulation parameter ϕ of 750 MV.

Table 2
Uncertainties in Source Abundances Derived from CRIS 2009–10 Observations

1	2 Source Abundance	3 Statistical Uncertainty	4 Systematic Measurement	5 Modulation	6 Partial Cross Sections	7 Total Cross Sections	8 Escape mfp	9 Total Statistical & Systematic	10 Statistical & Systematic if Partials Uncorrelated
$_{6}$C	3677.3	8.5	53.8	41.3	62.8	15.6	72.3	118.6	107.4
$_{7}$N	256.4	4.4	16.2	11.4	171.3	18.9	32.2	176.5	139.7
$_{8}$O	4837.3	8.9	64.3	41.2	40.2	25.6	44.0	100.6	93.3
$_{10}$Ne	511.0	3.5	10.5	0.6	55.5	6.1	10.2	57.9	29.0
$_{11}$Na	37.2	1.6	2.4	1.7	24.9	3.3	3.3	25.6	15.7
$_{12}$Mg	1111.2	4.5	17.1	1.5	21.6	2.0	5.1	28.5	21.7
$_{13}$Al	103.9	1.8	2.9	1.6	18.4	2.4	2.1	19.0	14.5
$_{14}$Si	1000.0	4.2	14.3	0.0	0.0	0.0	0.0	14.9	14.9
$_{16}$S	128.8	1.8	2.7	1.0	18.3	3.1	1.6	19.0	6.6
$_{18}$Ar	18.6	1.2	1.2	0.9	19.1	3.1	1.7	19.5	7.1
$_{20}$Ca	81.2	1.9	3.0	2.3	34.6	5.7	2.6	35.4	15.4
$_{26}$Fe	1037.3	4.3	15.3	11.6	6.2	2.6	8.5	22.4	22.1
$_{27}$Co	4.4	0.4	0.1	0.1	0.4	0.1	0.0	0.6	0.5
$_{28}$Ni	57.3	1.0	0.9	0.6	1.0	0.1	0.5	1.9	1.7

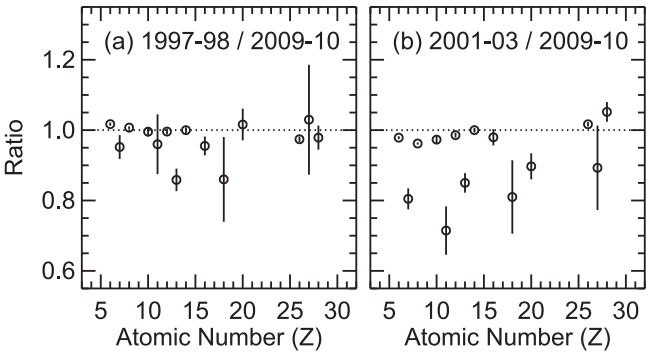

Figure 3. Comparison of various source abundances derived from CRIS data, with 1σ (i.e., one standard deviation) statistical uncertainties only. (Note the suppressed zero.) (a) Abundances derived from the 1997 December 5–1998 April 20 solar minimum over those derived from the 2009 March 23–2010 January 13 solar minimum. (b) Abundances derived from the 2001 May 1–2003 September 1 solar maximum over those derived from the 2009 March 23–2010 January 13 solar minimum.

Those HEAO3-C2 data were at energies 0.6–35 GeV/nucleon, higher than the energies of *ACE*-CRIS data.

The left section of Table 3 lists the source abundances as derived by Engelmann et al. (1990) from their HEAO3-C2 data, both with statistical uncertainties only and with their combination of uncertainties due to statistics and due to their estimate of systematic uncertainties resulting from cross-section uncertainties. The next section of Table 3 shows source abundances derived by us from the same HEAO3-C2 data, using the methods and model we applied to our CRIS data.

We note in Figure 5(a) significant differences between these two sets of source abundances, derived from the same observed data. While Figure 5(a) includes only statistical uncertainties resulting from the observed statistics, Table 3 demonstrates that the differences for many elements significantly exceed the combined statistical and systematic uncertainties assigned by Engelmann et al. We attribute these differences to differences between the propagation and modulation models used by Engelmann et al. in (1990) and those used by us today. Most particularly, the partial interaction cross sections in our calculation made extensive use of measured cross sections published since 1990 (Lave 2012). Furthermore, Engelmann et al. used a different form of the energy dependence of the escape mean free path than used by us.

The rightmost section of Table 3 duplicates the source abundances in the rightmost column of Table 1 with the addition of the systematic uncertainties estimated in Table 2—the best source abundances we have derived from our CRIS data. Figure 5(b) compares the source abundances derived by Engelmann et al. (1990) from their HEAO3-C2 data with those we derived from the CRIS data. We note differences substantially exceeding statistical uncertainties for many of the elements. The HEAO3-C2 data for Ne and lighter elements were for energies 0.6–35 GeV/nucleon, while those for elements heavier than Ne were for energies 0.8–35 GeV/nucleon. We expect that this small difference in energy intervals would have a negligible effect on the derived source abundances.

Although those HEAO3-C2 data were taken at a time when solar modulation was intermediate between minimum and maximum, for most of these energies solar modulation is a small to negligible effect. The CRIS data were at lower energies, 50–550 MeV/nucleon, where solar modulation can be significant; however, the level of modulation during the 2009–10 period was remarkably low. Figure 5(c) compares the source abundances we derived from the *HEAO3* data of Engelmann et al. (1990) with those we derived from the CRIS data. We again note differences substantially exceeding statistical uncertainties for many of the elements. Thus, we attribute the difference between our derived abundances from *HEAO3* data and from the 2009–10 CRIS solar minimum primarily to systematic uncertainties in our interstellar propagation model—some combination of uncertainties in the energy dependence of interaction cross sections and in the energy dependence of the model of containment of cosmic rays in the Galaxy. We note that the abundances relative to Si for elements heavier than Si are generally greater from CRIS than from HEAO3-C2, and abundances for elements lighter than Si are generally less from CRIS than from HEAO3-C2. This trend could be related to differences in the rigidity dependence of the interstellar pathlength in our model.

Another set of elemental source abundances comes from the COSPIN/HET instrument on the *Ulysses* spacecraft (DuVernois & Thayer 1996). That instrument measured cosmic rays in the energy interval 40–450 MeV/nucleon, very similar to the energy

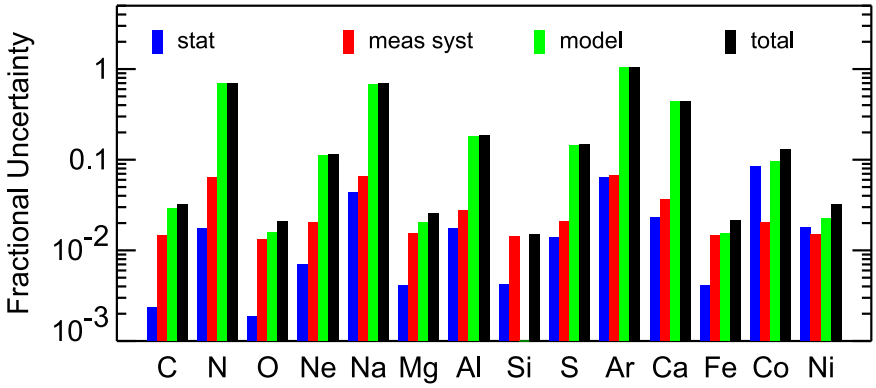

Figure 4. Fractional uncertainty in source abundances derived from the CRIS data from the 2009–10 solar minimum. The leftmost (blue) bar is from column 3 of Table 2. The next (red) bar is from column 4. The next (green) bar is from the quadratic sum of columns 5–8. The rightmost (black) bar is from column 9.

interval of CRIS. They reported measurements over the period from the launch of *Ulysses* in 1990 October through the middle of 1995, thus including a wide range of solar modulation levels. Unlike *HEAO3* and *ACE*, which were always in the ecliptic at 1 au from the Sun, *Ulysses* with perihelion at 1.35 au spent most of its time farther from the Sun, out to aphelion at 5.4 au, and was in an orbit nearly perpendicular to the ecliptic. They modeled the heliospheric modulation as a spherically symmetric field with a time-varying potential determined by the high-energy helium flux at the *IMP-8* satellite. In deriving source abundances they combined their data with data from above 800 MeV/nucleon from HEAO3-C2. The third section of Table 3 shows cosmic-ray source abundances reported by DuVernois & Thayer (1996) with uncertainties including both statistical and systematic uncertainties. (They did not report statistical or systematic uncertainties separately.) Comparison between their source abundances and our CRIS 2009–10 solar-minimum abundances (Figure 5(d)) again show some disagreements, which could be the result of differences in treatment of solar modulation and/or of cross sections used in the interstellar propagation.

Most recently, Cummings et al. (2016) have reported measurements from *Voyager 1* during the period from late 2012 to mid-2015, when the spacecraft was in the local interstellar medium (LISM). These data were at similar energies at the spacecraft to the energies of our *ACE*-CRIS data. (However, due to adiabatic energy loss during cosmic-ray transport through the heliosphere, the cosmic rays observed by *ACE*-CRIS had energies in the interstellar medium higher than the energies of most of the cosmic rays observed by *Voyager 1*.) Using those *Voyager* data, along with earlier data from *ACE*-CRIS (George et al. 2009), as well as the HEAO3-C2 data and data at higher energy from CREAM (Yoon et al. 2011), Cummings et al. (2016) derived source abundances using a leaky-box model similar to the interstellar model we used to find source abundances from our CRIS data, and they also derived source abundances using three versions of the GALPROP propagation model. All four of these propagations gave similar results for the elements considered in this CRIS paper. While they derived their best-estimate source by averaging the four calculated sources, we have selected their GALPROP Distributed Reacceleration (DR) model results for tabulating here because it listed statistical uncertainties derived in a similar way to the other models listed in Table 3. Furthermore, of the three GALPROP models used in Cummings et al. the GALPROP DR model was statistically favored. These results are shown in Table 3, and comparison between these source abundances and our CRIS 2009–10 solar-minimum source abundances are shown in Figure 5(e).

The differences among these various derived elemental source abundances point to systematic uncertainties that remain to be addressed. An examination of isotopic source abundances, which is planned for a later paper, is expected to resolve at least some of these uncertainties.

5. Discussion

Rauch et al. (2009) and Murphy et al. (2016) used their source abundances from the TIGER and the SuperTIGER instruments respectively for elements with $Z \geqslant 26$, combined with source abundances derived by Engelmann et al. (1990) for elements with $Z \leqslant 26$, to show that the cosmic-ray source is best understood as a mix of approximately 80% material of solar system composition and 20% outflow and ejecta from massive stars, with refractory elements accelerated preferentially by a factor of approximately four over volatile elements. A forthcoming paper (Binns et al. 2018) will report CRIS results from ~20 years of data for $Z \geqslant 28$; a preliminary version of those $Z \geqslant 28$ CRIS results appeared at the 2013 International Cosmic Ray Conference (Binns et al. 2013). Combining that paper's results with the CRIS source abundances for $Z \leqslant 28$ from this paper shows essentially the same features as seen by Rauch et al. and Murphy et al.—a consistent picture when the GCR source is compared with a solar system/Massive-Star-Material mix, and approximately four-to-one preferential acceleration of refractory over volatile elements. Both the TIGER and SuperTIGER observations and those of Engelmann et al. were for cosmic rays of about the same energies outside the atmosphere, >~0.8 GeV/nucleon, while the CRIS data reported in this paper and in the forthcoming paper (Binns et al. 2018) are for energies <0.55 GeV/nucleon. Thus, the CRIS results confirm the earlier conclusions of preferential acceleration of refractory elements and acceleration in OB associations.

We note that a separate CRIS study, looking at the abundance of the rare radioactive isotope ^{60}Fe (Binns et al. 2016), also is consistent with cosmic-ray acceleration in OB associations.

NASA grants NNX08AI11G and NNX13AH66G supported the work performed at the California Institute of Technology, the Jet Propulsion Laboratory, and Washington University in St. Louis. The work done at Goddard Space Flight Center was funded by NASA through the *ACE* Project. We thank Nasser

Table 3
Source Abundance Comparisons

	Engelmann et al. Source from HEAO-C2 data			Our Source from HEAO-C2 Data	DuVernois & Thayer Source Statistical & Systematic			Cummings et al. GALPROP DR Source		CRIS Source from Table 2		
		±stat	±stat & syst			+	−	mean	stat		±stat	±stat & syst
$_{6}$C	4249	31	121	4466.5	4474	256	241	4020	32.3	3677.3	8.5	118.6
$_{7}$N	254	8	88	393.7	342	28	28	337	17	256.4	4.4	176.5
$_{8}$O	5263	26	56	5088.7	5263	277	277	4990	38.7	4837.3	8.9	100.6
$_{10}$Ne	580	11	34	517.9	580	61	61	576	12	511.0	3.5	57.9
$_{11}$Na	32.3	1.5	12.6	31.8	32.4	13.0	7.7	38.8	2.0	37.2	1.6	25.6
$_{12}$Mg	1038	8	26	1091.0	1080	40	40	1110	18.3	1111.2	4.5	28.5
$_{13}$Al	77.8	2.6	14.6	77.0	77.8	13.0	10.0	102	2.2	103.9	1.8	19.0
$_{14}$Si	1000	3.6	13	1000.0	1000			1000	9.8	1000.0	4.2	14.9
$_{16}$S	131	3	9	130.7	131	20	20	133	5.4	128.8	1.8	19.0
$_{18}$Ar	22.3	1.6	6.3	13.6	22.3	12	8	20.8	2.9	18.6	1.2	19.5
$_{20}$Ca	60.1	2.2	9.3	43.8	65	12	8	64	3.9	81.2	1.9	35.4
$_{26}$Fe	1008	12	19	996.4	970	240	360	1090	12.4	1037.3	4.3	22.5
$_{27}$Co	1.9	0.6	0.6	2.0	2.4	2.2	2.2	2.0	0.2	4.4	0.4	0.6
$_{28}$Ni	56.8	2	2.2	56.0	51	14	14	59.9	1.9	57.3	1.0	1.9

Barghouty for his private communication of updated partial interaction cross sections of protons on heavy nuclei, and we thank Christina Cohen for her editorial assistance in preparing this manuscript.

Appendix A
Derivation of Source Abundances from Observations

For the purposes of deriving GCR source composition, we separated elements into two groups. The first group consisted of elements having source abundances large enough to allow them to be reliably determined from the composition measured near Earth when systematic uncertainties in the parameters of the propagation model are taken into account. For these elements there is no difficulty due to the model uncertainties leading to unphysical, negative source abundances. Based on prior work and on our own calculations, we assigned the following 14 elements to this group: C, N, O, Ne, Na, Mg, Al, Si, S, Ar, Ca, Fe, Co, Ni.

The remaining elements between C and Ni, which have sizable secondary fractions that interfere with reliably determining their source abundances, were assigned to the second group. In order to account for the fact that these group 2 elements contribute secondaries to the observed spectra of lighter elements in both groups, we adopted assumed ratios in the source relative to a nearby reference element in group 1. In cases where there were several possible reference elements that could be used, we chose one that has similar volatility in order to minimize uncertainties due to fractionation effects. In addition, for elements in both groups, we adopted assumed isotopic source compositions. With the exception of ^{22}Ne, we assumed that the composition is the same as that of primordial solar system material (Lodders et al. 2009). For ^{22}Ne, we adopted the GCR source ratio ^{22}Ne/^{20}Ne derived by Binns et al. (2005). Table 4 lists all of the assumptions we used to calculate the source composition from the abundances of the elements in group 1.

In order to calculate source abundances for the group 1 elements, we first did a series of propagation and solar modulation calculations, each one using the source composition listed in one of the rows of Table 4. These contain unit abundance of one fitted element together with any "scaled elements" listed in column 3 of the same row with the indicated abundance relative to the fitted element. Both fitted and scaled elements were partitioned into the isotope percentages that are listed. Each of these calculations resulted in a set of near-Earth spectra, including both nuclides included in the source and fragmentation products they produce during transport through the interstellar medium. Besides the source composition, the calculated near-Earth spectra depend on a number of other parameters (source spectral shape, energy-dependent escape mean free path, various cross sections and half-lives, level of solar modulation, etc.). All of these parameters (other than the source abundances) were previously determined. We employed a leaky-box propagation model and a spherically symmetric modulation using parameters that Lave et al. (2013) derived from *ACE*/CRIS measurements of secondary-to-primary ratios as a function of energy.

The source abundances of the fitted elements are constrained by a set of near-Earth measurements of spectral intensities. We let $J_i \pm \sigma_i$ denote the measured intensity and associated uncertainty for the element Z_i at energy per nucleon ϵ_i. In the *ACE*/CRIS data set, we have measurements at seven Z-dependent energy-per-nucleon values. Thus, the total number of data points constraining the fit of $n = 14$ source abundances was $N = 7 \times 14 = 98$.

We denote by q_j the source abundance of the fitted element Z_j and by $\varphi^i_j(\epsilon_i)$ the calculated near-Earth intensity spectrum of the element Z_i obtained by propagating/modulating the source spectrum containing unit abundance of the element Z_j, together with contributions from any group 2 elements scaled from it (Table 4). For a given set of group 1 source abundances, q_1, q_2, … q_n, near-Earth spectra of all group 1 elements can be obtained by adding up the contributions from the n individual propagation/modulation calculations,

$$\varphi^i(\epsilon) = \sum_{j=1}^{n} q_j \varphi^i_j(\epsilon). \quad (1)$$

This function, which we used to fit the measured near-Earth intensities, is linear in the n source abundances, so the fitting of these values is a standard linear least-squares problem. The

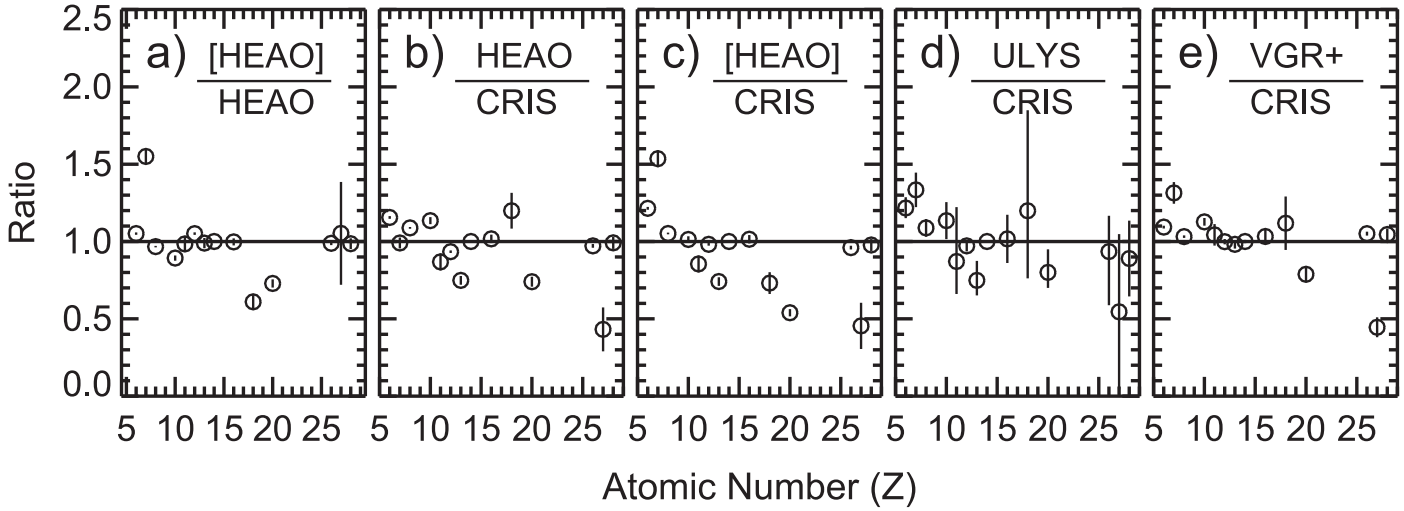

Figure 5. Ratios of various derived source abundances to one another. (a) Abundances derived by our calculation from *HEAO3* data of Engelmann et al. (1990; denoted by [HEAO]) over those derived by Engelmann et al. (1990) from the same data (denoted by HEAO). (The error bars come from only the statistical uncertainties assigned by Engelmann et al. to their derived source abundances.) (b) Abundances derived by Engelmann et al. (1990) over those derived by us from CRIS 2009–10 data. (The error bars come from combining only the statistical uncertainties of the two results.) (c) Abundances derived by our calculation from *HEAO3* data of Engelmann et al. (1990) [HEAO] over those derived by us from CRIS 2009–10 data. (Error bars come from combining only the statistical uncertainties of the two results.) (d) Abundances derived by DuVernois & Thayer (1996) using their *Ulysses* data and data from HEAO-C2 over those derived by us from CRIS data of 2009–10. (Error bars come from combining the statistical uncertainties of the CRIS results and the only uncertainties given by DuVernois & Thayer (1996), which include systematic uncertainties.) (e) Abundances derived by Cummings et al. (2016) using their *Voyager 1* data collected in the local interstellar medium, together with data sets from a number of near-Earth spacecraft over those derived by us from CRIS data of 2009–10 The source abundances from the GALPROP DR model in Cummings et al. were used for this comparison.

source abundances $q_1 \ldots q_n$ were obtained by minimizing the χ^2 function defined as

$$\chi^2 = \sum_{i=1}^{N} w_i \left[J_i - \sum_{j=1}^{n} q_j \varphi^i_j(\epsilon_i) \right]^2 \tag{2}$$

with respect to these source abundances using weights defined as $w_i = 1/\sigma_i^2$.

As discussed in various texts (e.g., Bevington 1969; Bonamente 2017), the solution involves constructing a matrix $\boldsymbol{M}$ with elements

$$M_{jk} = \sum_{i=1}^{N} w_i \varphi^i_j(\epsilon_i) \varphi^i_k(\epsilon_i) \tag{3}$$

and a vector $\boldsymbol{V}$ with elements

$$V_j = \sum_{i=1}^{N} w_i \varphi^i_j(\epsilon_i) J_i. \tag{4}$$

Multiplying $\boldsymbol{M}^{-1}$, the inverse of $\boldsymbol{M}$, into $\boldsymbol{V}$ yields the vector of coefficients, which are the desired source abundances $q_1 \ldots q_n$. The uncertainties in the source abundances are obtained from the diagonal elements of the inverse matrix as

$$\sigma_{q_j} = \sqrt{(M^{-1})_{jj}}. \tag{5}$$

Applying this procedure with the σ_i values equal only to the statistical uncertainties in the measured spectral intensities, we obtained the source compositions and statistical uncertainties shown in Table 1. Columns 2 and 3 of Table 2 are identical with the 2009–10 section of Table 1. A similar calculation with the σ_i values equal only to the systematic uncertainties in the measurements yielded the values in column 4 of Table 2. The source abundances obtained from this latter calculation agreed with those shown in column 2 to within 7% for Ar, 4% for Co, and 3% for the other fitted elements.

Appendix B
Uncertainties due to Uncorrelated Cross-section Uncertainties

In column 6 of Table 2 we showed the uncertainties in derived source abundances caused by fully correlated errors in partial cross sections at an assumed level of 20%. If the errors were completely uncorrelated, the associated uncertainties in the source abundances would be smaller. In this appendix we derive the ratio of these uncertainties for the uncorrelated case to those for the fully correlated case, which allows us to calculate source abundance uncertainties given in column 10 of the table.

The leaky-box equation relating GCR source spectra (q_i) and equilibrium interstellar spectra (φ_i) can be written (Meneguzzi et al. 1971) as

$$q_i = -\sum\nolimits_j \varphi_j \frac{\sigma^*_{ji}}{M^*} + \varphi_i \left(\frac{\sigma^*_i}{M^*} + \frac{1}{\Lambda^i_{\rm esc}} \right) - \frac{d}{d\epsilon}(w_i \varphi_i), \tag{6}$$

with effective partial cross sections, effective total cross sections, and effective ISM target masses defined for convenience as $\sigma^*_{ji} \equiv \sigma_{{\rm H}ij} + (n_{\rm He}/n_{\rm H})\sigma_{{\rm He}ij}$, $\sigma^*_i \equiv \sigma_{{\rm H}i} + (n_{\rm He}/n_{\rm H})\sigma_{{\rm He}i}$, $M^* \equiv M_{\rm H} + (n_{\rm He}/n_{\rm H})M_{\rm He}$. Other symbols are as defined in George et al. (2009).

Fractional uncertainties, f, in the effective partial cross sections produce uncertainties in the derived source abundances denoted by $\delta q_i^{\rm cor}$ and $\delta q_i^{\rm uncor}$ for the cases when the cross-section uncertainties are fully correlated (cor) and fully uncorrelated (uncor) with

$$\delta q_i^{\rm cor} = f \sum\nolimits_j \varphi_j \frac{\sigma^*_{ji}}{M^*} \tag{7}$$

Table 4
Assumed Composition of Individually Propagated Sources

j	Fitted Element	Scaled Elements	Source Isotope Percentages	Reference
1	C = 1		^{12}C = 98.889%, ^{13}C = 1.111%	1
2	N = 1		^{14}N = 99.634%, ^{15}N = 0.366%	1
3	O = 1		^{16}O = 99.763%, ^{17}O = 0.037%, ^{18}O = 0.200%	1
		F = 5.12×10^{-5}	^{19}F = 100%	1
4	Ne = 1		^{20}Ne = 72.0%, ^{21}Ne = 0.173%, ^{22}Ne = 27.8%	2
5	Na = 1		^{23}Na = 100%	1
6	Mg = 1		^{24}Mg = 78.992%, ^{25}Mg = 10.003%, ^{26}Mg = 11.005%	1
7	Al = 1		^{27}Al = 100%	1
8	Si = 1		^{28}Si = 92.230%, ^{29}Si = 4.683%, ^{30}Si = 3.087%	1
9	S = 1		^{32}S = 95.018%, ^{33}S = 0.75%, ^{34}S = 4.215%, ^{36}S = 0.017%	1
		P = 1.97×10^{-2}	^{31}P = 100%	1
		Cl = 1.23×10^{-2}	^{35}Cl = 75.771%, ^{37}Cl = 24.229%	1
10	Ar = 1		^{36}Ar = 84.595%, ^{38}Ar = 15.381%, ^{40}Ar = 0.024%	1
11	Ca = 1		^{40}Ca = 96.941%, ^{42}Ca = 0.647%, ^{43}Ca = 0.135%, ^{44}Ca = 2.086%, ^{46}Ca = 0.004%, ^{48}Ca = 0.187%	1
		K = 6.23×10^{-2}	^{39}K = 93.132%, ^{40}K = 0.147%, ^{41}K = 6.721%	1
12	Fe = 1		^{54}Fe = 5.845%, ^{56}Fe = 91.754%, ^{57}Fe = 2.1191%, ^{58}Fe = 0.2819%	1
		Sc = 4.06×10^{-5}	^{45}Sc = 100%	1
		Ti = 2.91×10^{-3}	^{46}Ti = 8.249%, ^{47}Ti = 7.437%, ^{48}Ti = 73.72%, ^{49}Ti = 5.409%, ^{50}Ti = 5.185%	1
		V = 3.37×10^{-4}	^{50}V = 0.2497%, ^{51}V = 99.7503%	1
		Cr = 1.54×10^{-2}	^{50}Cr = 4.3452%, ^{52}Cr = 83.7895%, ^{53}Cr = 9.5006%, ^{54}Cr = 2.3647%	1
		Mn = 1.09×10^{-2}	^{55}Mn = 100%	1
		Cu = 6.38×10^{-4}	^{63}Cu = 69.174%, ^{65}Cu = 30.826%	1
		Zn = 1.53×10^{-3}	^{64}Zn = 48.63%, ^{66}Zn = 27.9%, ^{67}Zn = 4.1%, ^{68}Zn = 18.75%, ^{70}Zn = 0.62%	1
		Ga = 4.32×10^{-5}	^{69}Ga = 60.108%, ^{71}Ga = 39.892%	1
		Ge = 1.36×10^{-4}	^{70}Ge = 21.234%, ^{72}Ge = 27.662%,^{73}Ge = 7.717%, ^{74}Ge = 35.943%, ^{76}Ge = 7.444%	1
13	Co = 1		^{59}Co = 100%	1
14	Ni = 1		^{58}Ni = 68.0769%, ^{60}Ni = 26.2231%, ^{61}Ni = 1.1399%, ^{62}Ni = 3.6345%, ^{64}Ni = 0.9256%	1

References. 1. Lodders et al. (2009) 2. ^{21}Ne/^{20}Ne from Lodders et al. (2009), ^{22}Ne/^{20}Ne from Binns et al. (2005).

and

$$\delta q_i^{\rm uncor} = f\left[\sum_j \left(\varphi_j \frac{\sigma^*_{ji}}{M^*}\right)^2\right]^{1/2}. \quad (8)$$

Thus, the ratio of the source abundance uncertainty due to fully uncorrelated cross-section uncertainties to that due to fully correlated cross-section uncertainties is simply given by

$$\frac{\delta q_i^{\rm uncor}}{\delta q_i^{\rm cor}} = \frac{\left[\sum_j (\varphi_j \sigma^*_{ji})^2\right]^{1/2}}{\sum_j \varphi_j \sigma^*_{ji}}. \quad (9)$$

These calculations are essentially what was described by Hinshaw & Wiedenbeck (1983).

The source abundance uncertainties in the fully correlated case, $\delta q_i^{\rm cor}$, are easily evaluated by varying all of the partial cross sections by the same factor, repeating the propagation calculations used to derive source abundances, and taking differences from the baseline case that uses nominal cross sections. To obtain source abundance uncertainties in the fully uncorrelated case, $\delta q_i^{\rm uncor}$, one can just multiply the results obtained in the fully correlated case by the factor given in Equation (9). Note that the quantities in Equation (9) are energy-dependent. If the leaky-box equation (Equation (6)) is rigorously satisfied and the source abundances are energy-independent, as assumed, the ratio in Equation (9) would not depend on energy. In reality, it does have some energy dependence. We have evaluated this ratio at an interstellar energy obtained by adding typical values of the measurement energy and the energy lost in penetrating to near Earth under solar-minimum conditions.

In the above discussion, uncertainties were considered in the values of the effective decayed partial cross sections. Thus, it was implicitly assumed that the uncertainties in $\sigma_{{\rm H}ij}$ and $\sigma_{{\rm He}ij}$ for the same ji are fully correlated. In addition, it was assumed that uncertainties in all of the undecayed cross sections that get summed (taking branching ratios into account) to give a particular decayed cross section are fully correlated. The effect of cross-section uncertainties that are uncorrelated between H and He targets and/or among different reactions that contribute to the same decayed cross section can be calculated using simple extensions of Equation (9). However, the additional effort required to use a more elaborate result than Equation (9) hardly seems justified given the paucity of information available about the cross-section uncertainties and their correlations.

Typically, source abundances are reported as ratios to some reference element. Unless that reference element is entirely primary, its derived source abundance will also vary when one does a propagation calculation with all the partial cross sections modified by the same factor. If this variation is ignored in calculating uncertainties in the derived abundance ratios, the uncertainties will be systematically underestimated because changing all of the cross sections by the same factor will change the numerator and the denominator in the same direction. If the element chosen for normalization is dominantly primary, the inaccuracy that this introduces should be negligible for elements for which partial cross-section uncertainties are a significant contributor to the overall uncertainty in the derived source abundance ratio. We have normalized to Si, which has an estimated secondary contribution of ~7%.

ORCID iDs

M. H. Israel https://orcid.org/0000-0002-8104-208X
M. E. Wiedenbeck https://orcid.org/0000-0002-2825-3128
W. R. Binns https://orcid.org/0000-0001-6110-3407
E. R. Christian https://orcid.org/0000-0003-2134-3937
A. C. Cummings https://orcid.org/0000-0002-3840-7696
G. A. de Nolfo https://orcid.org/0000-0002-3677-074X
R. A. Mewaldt https://orcid.org/0000-0003-2178-9111
E. C. Stone https://orcid.org/0000-0002-2010-5462

References

Bevington, P. B. 1969, Data Reduction and Error Analysis for the Physical Sciences (New York: McGraw-Hill)
Binns, W. R., Christian, E. R., Cummings, A. C., et al. 2013, ICRC (Rio de Janeiro), 1, 319
Binns, W. R., Israel, M. H., Christian, E. R., et al. 2016, Sci, 352, 677
Binns, W. R., Wiedenbeck, M. E., Arnould, M., et al. 2005, ApJ, 634, 351
Binns, W. R., Wiedenbeck, M. E., Arnould, M., et al. 2007, SSRv, 130, 439
Binns, W. R., Wiedenbeck, M. E., Christian, E. R., et al. 2018, Elemental Composition at the Cosmic-Ray Source derived from the ACE-CRIS Instrument II: $_{29}$Cu to $_{40}$Zr, in press
Bonamente, M. 2017, Statistics and Analysis of Scientific Data (2nd ed.; New York: Springer)
Cummings, A. C., Stone, E. C., Heikkila, B. C., et al. 2016, ApJ, 831, 18
Davis, A. J., Mewaldt, R. A., Binns, W. R., et al. 2000, in AIP Conf. Ser. 528, Accleration and Transport of Energetic Particles Observed in the Heliosphere, ACE-2000 Symposium, ed. R. A. Mewaldt et al. (Melville, NY: AIP), 421
DuVernois, M. A., & Thayer, M. R. 1996, ApJ, 465, 982
Engelmann, J. J., Ferrando, P., Soutoul, A., et al. 1990, A&A, 233, 96
Fisk, L. A. 1971, JGR, 76, 221
George, J. S., Lave, K. A., Wiedenbeck, M. E., et al. 2009, ApJ, 696, 1666
Gleeson, L. J., & Axford, W. I. 1968, ApJ, 154, 1011
Goldstein, M. L., Fisk, L. A., & Ramaty, R. 1970, PhRvL, 25, 832
Higdon, J. C., & Lingenfelter, R. E. 2003, ApJ, 590, 822
Hinshaw, G. F., & Wiedenbeck, M. E. 1983, Proc. ICRC (Bangalore India), 9, 263
Lave, K. A. 2012, PhD thesis, Washington Univ. (http://openscholarship.wustl.edu/cgi/viewcontent.cgi?article=1706&context=etd)
Lave, K. A., Wiedenbeck, M. E., Binns, W. R., et al. 2013, ApJ, 770, 117
Lodders, K., Palme, H., & Gail, H.-P. 2009, LanB, 4B, 712
Meneguzzi, M., Audouze, J., & Reeves, H. 1971, A&A, 15, 337
Mewaldt, R. A., Davis, A. J., Lave, K. A., et al. 2010, ApJL, 723, L1
Murphy, R. P., Sasaki, M., Binns, W. R., et al. 2016, ApJ, 831, 148
Niebur, S. M., Scott, L. M., Wiedenbeck, M. E., et al. 2003, JGRA, 108, 8033
Rauch, B. F., Link, J. T., Lodders, K., et al. 2009, ApJ, 697, 2083
Soutoul, A., & Ptuskin, V. S. 1999, Proc. ICRC (Salt Lake City), 4, 184
Stone, E. C., Cohen, C. M. S., Cook, W. R., et al. 1998a, SSRv, 86, 285
Stone, E. C., Frandsen, A. M., Mewaldt, R. A., et al. 1998b, SSRv, 86, 1
Wiedenbeck, M. E., Binns, W. R., Cummings, A. C., et al. 2007, SSRv, 130, 415
Wiedenbeck, M. E., Davis, A. J., Leske, R. A., et al. 2005, Proc. ICRC (Pune India), 2, 277
Yoon, Y. S., Ahn, H. S., Allison, P. S., et al. 2011, ApJ, 728, 122